Redox Biology 57 (2022) 102493

Contents lists available at ScienceDirect

Redox Biology

journal homepage: www.elsevier.com/locate/redox

CircRAPGEF5 interacts with RBFOX2 to confer ferroptosis resistance by modulating alternative splicing of TFRC in endometrial cancer

Jun Zhang [a,1], Shuaijun Chen [b,1], Sitian Wei [a,1], Shuangshuang Cheng [a], Rui Shi [a], Rong Zhao [a], Wei Zhang [a], Qi Zhang [a], Teng Hua [a], Dilu Feng [a], Zhicheng Yu [a,**], Hongbo Wang [a,c,*]

[a] Department of Obstetrics and Gynecology, Union Hospital, Tongji Medical College, Huazhong University of Science and Technology, Wuhan, Hubei, 430022, China
[b] Department of Pathology, The Central Hospital of Wuhan, Tongji Medical College, Huazhong University of Science and Technology, Wuhan 430014, China
[c] Clinical Research Center of Cancer Immunotherapy, Wuhan, Hubei, 430022, China

ARTICLE INFO

Keywords:
Endometrial cancer
Ferroptosis
Alternate splicing
CircRAPGEF5
RBFOX2
TFRC

ABSTRACT

Endometrial cancer (EC) is one of the most common gynecological cancers. Ferroptosis is a newly identified form of cell death characterized by iron-dependent lipid peroxide accumulation. Circular RNAs (circRNAs) have emerged as critical regulators for cancer development. However, circRNA-mediated modulation of ferroptosis in EC is yet to be clarified. In this study, we found that circRAPGEF5 expression was elevated in EC tissues compared to the normal endometrial tissues. In vitro and in vivo functional analysis demonstrated that circRAPGEF5 facilitates rapid proliferation of EC cells. RNA binding protein fox-1 homolog 2 (RBFOX2), a splicing regulator, was identified as the protein interacts with circRAPGEF5. Further studies revealed that circRAPGEF5 can bind to the Fox-1 C-terminal domain of RBFOX2 and induces specific exon exclusion of TFRC through obstructing the binding of RBFOX2 to pre-mRNA. As a result, elevated levels of circRAPGEF5 lead to ferroptosis resistance via the decreased labile iron pool and attenuated lipid peroxide production in EC cells. Additionally, a series of gain- and loss-of-function experiments demonstrated that knocking down or overexpressing RBFOX2 reversed the effects of knocking down or overexpressing circRAPGEF5 in EC cells. Finally, it is revealed that circRAPGEF5 promote the formation of TFRC with exon-4 skipping and confer ferroptosis resistance in EC cells through the interaction with RBFOX2. Collectively, these findings provide new insight into the molecular mechanism in which circRNAs mediate mediates ferroptosis via modulating alternative splicing, and circRAPGEF5/RBFOX2 splicing axis could be a promising therapeutic target for treating EC.

1. Introduction

Endometrial cancer (EC) is one of the most common gynecological cancers, with more than 280,000 cases per year, worldwide [1,2]. ECs have long been divided into two types: type I and type II. Type I ECs are low-grade, estrogen-dependent tumors, whereas type II ECs are aggressive and estrogen-independent. Type I ECs account for more than 80% of uterine cancers and have a relatively good prognosis, with a 5-year survival rate of 80–85% following surgery. Type II ECs are usually characterized by early metastasis, high-grade malignancy, and poor prognosis, with a 5-year survival rate of only 35% [3]. Patients with advanced EC have a significantly shorter survival time and limited treatment options compared to patients with early EC. Some novel therapeutic strategies have been developed, such as lenvatinib plus pembrolizumab, that showed promising antitumor activity in patients with advanced EC. Despite these developments, the prognosis for advanced EC remains dismal [4,5]. Thus, a better understanding of the mechanisms underlying the progression of EC would be beneficial for further development of treatment.

Alternative splicing (AS), an important post-transcriptional process, is a key mechanism for modulating gene functions and gives rise to diverse messenger RNA (mRNA) isoforms via different arrangements of exons within precursor mRNAs [6]. AS plays a fundamental role in the expression of eukaryotic genes, and human cancers frequently exhibit

* Corresponding author Obstetrics and Gynecology, Union Hospital, Tongji Medical College, Huazhong University of Science and Technology, Wuhan, Hubei, 430022, China
** Corresponding author.
E-mail addresses: d202081746@hust.edu.cn (Z. Yu), drwanghb69@hust.edu.cn (H. Wang).
[1] These authors contributed equally to this work.

https://doi.org/10.1016/j.redox.2022.102493
Received 15 August 2022; Received in revised form 21 September 2022; Accepted 23 September 2022
Available online 26 September 2022

dysregulation of the splicing factor function and expression of cancer-specific splicing isoforms. This makes AS an important signature for tumor progression and therapy [7]. RNA-binding proteins (RBPs) play a critical role in cancer splicing and dysregulated RBP expression dramatically alters the cellular AS profiles, thus influencing tumor biology [8]. For instance, SRSF10 mediates the aberrant upregulation of exon 10-inclusive SREK1, an oncogenic driver in human hepatocellular carcinoma [9]. Another serine/arginine (SR)-rich protein, SRSF2, regulates AS to drive hepatocellular carcinoma development [10]. Pooja et al. reported that SF3B1 promotes endometrial cancer progression by regulating KSR2 RNA maturation [11]. However, the role of aberrant AS and splicing regulators in EC development have not been elucidated.

Circular RNAs (circRNAs) are a class of covalent, closed, and single-stranded RNA molecules generated by back-splicing or other RNA circularization mechanisms [12]. Unlike linear RNAs, circRNAs are not readily degraded by RNA exonucleases, which results in greater stability [13]. CircRNAs were originally considered byproducts of erroneous splicing with no specific functions. However, numerous studies have demonstrated that circRNAs contribute to the majority of biological processes, including the cell cycle, cell growth, and metastasis [14]. In most studies, circRNAs exert gene regulatory functions by serving as miRNAs sponges [12]. They also interact with RBPs to form RNA-protein complexes, which regulate the activities of associated proteins [15]. Partial circRNA molecules containing internal ribosome entry sites (IRESs) have proven to be translatable [16]. Notably, accumulating evidence has illustrated that circRNAs play a vital role in the growth and development of EC by sponging miRNAs [17–19]. This is an incomplete picture, and the regulatory functions of circRNAs in modulating AS in EC have yet to be fully defined.

2. Materials and methods

2.1. Patients and tissue specimen collection

A total of 30 EC tissues and 25 normal endometrial tissues were obtained from patients who underwent surgical procedures at the Department of Obstetrics and Gynecology at the Union Hospital of Tong Medical College (Wuhan, China). Detailed information is presented in Table 1. All specimens were snap-frozen in liquid nitrogen immediately after resection. All participants provided written informed consent, and the institutional review board of Tongji Medical College at Huazhong University of Science and Technology approved all study protocols.

Table 1
Clinicopathological features of 30 endometrial cancer patients and the expressions of circRAPGEF5Figure legends.

Parameters	Group	circ RAPGEF5 expression		P value
		High (>median)	Low (<median)	
Age at surgery				
	<60	7 (46.7%)	11 (73.3%)	0.264
	>60	8 (53.3%)	4 (26.7%)	
FIGO stage				
	StageI	4 (26.7%)	12 (80.0%)	0.026
	StageII	6 (40.0%)	1 (6.7%)	
	StageIII	4 (26.7%)	2 (13.3%)	
	StageIV	1 (6.7%)	0 (0%)	
Pathological type				
	Endometrioid	10 (66.7%)	14 (93.3%)	0.171
	Non-endometrioid	5 (33.3%)	1 (6.7%)	
Histological grade				
	G1	2 (13.3%)	10 (66.7%)	0.005
	G2	3 (20.0%)	3 (20.0%)	
	G3	10 (66.7%)	2 (13.3%)	
Lymph node metastasis				
	Absent	10 (66.7%)	13 (86.7%)	0.388
	Present	5 (33.3%)	2 (13.3%)	

2.2. Cell culture and treatment

The human endometrial cancer cell lines KLE, Ishikawa, HEC-1-A, HEC-1-B, and RL95-2 were obtained from the American Type Culture Collection (ATCC). KLE, RL95-2, and Ishikawa cells were maintained in DMEM/F12 medium containing 10% fetal bovine serum (FBS) (Gibco), and HEC-1-A cells were maintained in McCoy's 5A medium containing 10% FBS. HEC-1-B cells were maintained in MEM containing 10% FBS. Cells were cultured in a 5% CO2 incubator at 37 °C.

To construct circular circRAPGEF5 overexpression plasmids, human circRAPGEF5 and complementary DNA (cDNA) were synthesized by Genomeditech (Shanghai, China) and cloned into the GPLVX-Laccase2-MCS-Puro Vector (GM-9457). The small hairpin RNAs (shRNAs) of circRAPGEF5 and RBFOX2 were synthesized and cloned into the PGMLV-HU6-MCS-CMV-PGK-Puro vector by Genomeditech (Shanghai, China). Human RBFOX2 (NM_014309.4) and transferrin receptor protein 1 (TFRC, NM_003234) cDNAs were amplified by PCR and cloned into a pcDNA 3.1 expression vector (Genomeditech, Shanghai, China). The shRNA sequences used are listed in Supplementary Table S1. We established stable cell lines with circRAPGEF5 knockdown or overexpression using a lentiviral–mediated delivery system at a multiplicity of infection (MOI) of 30 using polybrene. Cells were selected using 2 μg/mL puromycin for 48 h to establish stable cell lines. The empty vector and scramble shRNA were used as controls. For plasmid transfection, KLE and Ishikawa cells were cultured in six-well plates and transfected with 2 μg of expression plasmid using Lipofectamine 3000 (Invitrogen, CA, USA), according to the manufacturer's instructions. Protein lysates and total RNA were collected 72 h after transfection to verify transfection efficiency using western blotting and qPCR.

2.3. RNA isolation and quantitative real-time PCR (qRT-PCR)

Total RNA was isolated from the cells or tissues using TRIZOL® reagent (Takara, Otsu, Japan), according to the manufacturer's instructions. Total RNA was reverse-transcribed into cDNA using the Hiscript QRT SuperMix (Vazyme, Nanjing, China). Real-time PCR analyses were performed on a CFX Connect Real-Time PCR Detection System (Bio-Rad, Hercules, CA, USA) using Universal SYBR Green Fast qPCR Mix (Abclonal, Wuhan, China). GAPDH was selected as an internal reference for normalization of the qPCR results, and qualified expression was calculated using the 2(-ΔΔCT) method. The primers used are listed in Supplementary Table 1.

2.4. Nuclear and cytoplasmic extraction, RNase R and actinomycin D treatment

Nuclear and cytoplasmic RNAs were extracted using a nuclear and cytoplasmic RNA purification kit (Fisher Scientific, AM1921). For RNase R treatment, 1 μg of total RNA was incubated for 15 min at 37 °C with or without 3 U of RNase R (Epicentre Technologies, Madison, WI). For actinomycin D (ActD) treatment, 5 μg/mL ActD (Sigma-Aldrich, USA) was used to block transcription in the EC cells, which were harvested after 0, 4, 8, 12, and 24 h of treatment.

2.5. RNA pull-down assays and RNA immunoprecipitation (RIP)

A biotin-labeled oligonucleotide probe targeting the junction site of circRAPGEF5 was synthesized by RiboBio (Guangzhou, China) (Supplementary Table 1). RNA pull-down assays were conducted using the Pierce™ Magnetic RNA-Protein Pull-Down Kit (20164, Thermo Scientific), according to the manufacturer's instructions. The resulting circRAPGEF5-protein complexes were analyzed by immunoblotting or mass spectrometry.

RIP experiments were performed using a Magna RIP RNA-Binding Protein Immunoprecipitation Kit (Millipore, Bedford, MA, USA) according to the manufacturer's instructions. Cell lysates were incubated

with 5 μg of primary antibodies against Argonaute RISC Catalytic Component 2 (AGO2) (Cell Signaling Technologies, #2897), RBFOX2 (ab264154, Abcam, Cambridge, UK), and FLAG (M20008, Abmart). The controls used were mouse or rabbit IgG.

2.6. Silver staining and mass spectrometry (MS) analysis

After 75 min of electrophoresis (120V), silver staining of the gel was performed using a Fast Silver Stain Kit (P0017S, Beyotime) according to the manufacturer's instructions. MS was performed by SpecAlly Life Technology Co., Ltd. (Wuhan, China). In brief, the immobilized magnetic bead-bound complexes were cleaned and digested using sequencing-grade modified trypsin. After extraction and purification, the peptide samples were identified by mass spectrometry (Q Exactive, Thermo Finnigan, US). The acquired raw mass spectrometric data were searched using MaxQuant software (V1.6.2.10). The human reference proteome database from UniProt was used.

2.7. Fluorescent in situ hybridization (FISH)

A Cy3-labeled circRAPGEF5 FISH probe was synthesized by RiboBio (Guangzhou, China) and circRAPGEF5 FISH was conducted using a Ribo FISH kit (C10910, RiboBio). Briefly, 10^4 EC cells were seeded in 24-well plates and cultured overnight. The following day, cells were fixed, permeabilized, and then incubated in probes hybridization buffer containing 4 nM FISH probes overnight at 37 °C. After thorough washing, nuclei were counterstained with DAPI (C1002, Beyotime). Images were acquired using a fluorescence microscope (Nexcope NE930, Ningbo, China).

2.8. Immunofluorescence

For immunofluorescence staining, EC cells (2×10^4) were fixed in 4% paraformaldehyde 24 h after seeding. Cells were permeabilized with 0.5% Triton X-100 for 10 min, blocked with 5% BSA for 1 h and incubated in 5% BSA with the indicated antibodies at 4 °C overnight. FITC-conjugated AffiniPure goat anti-rabbit IgG (H + L) (BOSTER, BA1105, 1:200) was used as the secondary antibody. DAPI (C1002, Beyotime) was used to stain nuclei. Images were taken by confocal microscopy (LSM800, Zeiss).

2.9. Western blot

Whole cell lysates were prepared using RIPA buffer (G2002, Servicebio) containing protease inhibitors (B14001, Bimake). Proteins were denatured using 5 × loading buffer.

(AR1112, BOSTER), and boiled for 5 min. Equal quantities of total protein were separated with SDS-PAGE and transferred to PVDF membranes (ISEQ00010, Merck Millipore). The membranes were then blocked with 5% non-fat dry milk in 0.1% TBST for 1 h. Primary antibodies were incubated overnight at 4 °C, and corresponding secondary antibodies for 1 h at room temperature. Protein detection was performed using ECL detection reagent (BL520A, Biosharp) and ChemiDoc Imaging Systems (BioRad).

The primary antibodies used were against RBFOX2 (ab264154, Abcam), RAPGEF5(12556-1-AP, Proteintech), AGO2 (#2897, Cell Signaling Technologies), FLAG (M20008, Abmart), and GAPDH (AC002, Abclonal). Secondary antibodies used were HRP-conjugated secondary goat anti-mouse (AS003, Abclonal), goat anti-rabbit (AS014, Abclonal), HRP-conjugated AffiniPure Goat Anti-Mouse IgG Light Chain (AS062, Abclonal) and HRP-mouse anti-rabbit IgG light chain-specific (SA00001-7 L, Proteintech).

2.10. CircRNA identification

We obtained pairs of reads from an Illuminas HiSeq 4000 sequencer and the low-quality data were filtered from the sequencing data using Cutadapt software (v1.9.3). STAR software was used to align the reads to the reference genome (UCSC HG19), and DCC software was used to detect and annotate circRNA clusters. Annotations were performed using the circBase and circ2Trait disease databases. The EdgeR package in R software was used to calculate differentially expressed circRNAs based on normalized junction read counts. Differential expression of circRNAs was calculated using the following criteria: Log_2 (fold change) > 1.0 (or < -1.0) and P-value < 0.05 (Supplementary Table 2).

2.11. Analysis of alternative splicing

Total RNAs isolated from KLE cells transfected with sh-circRAPGEF5 or control shRNA were used to construct cDNA libraries. The final cDNA libraries were added to FLO MIN109 flow cells and analyzed on a PromethION platform at Biomarker Technology Company (Beijing, China). Transcript validation was performed using GFFcompare software with reference annotations. AS events including RI (Retained intron), SE (Skipping exon), A5 (Alternative 5′ splice-site), and A3 (Alternative 3' splice-site) were identified by the AStalavista tool. The percentage spliced in (PSI) score was used to measure the degree of alternative exon inclusion and is calculated as IR/(IR + ER), where IR represents inclusion reads and ER represents exclusion reads. Dysregulated alternative splicing events (Supplementary Table 3) were determined using the criteria of $P < 0.05$ and $| \Delta PSI | > 0.05$.

2.12. Cell proliferation assay

Cell proliferation assays were performed as described [19].

2.13. Cell viability assay

5×10^3 EC cells were seeded in 96-well plates and treated with media containing erastin (S7242, Selleck), RSL3 (S8155, Selleck), or DMSO for 12 h on the next day. These media were then discarded and replaced with 100 μL of complete medium containing 10 μL of CCK-8 reagent (Topscience, Shanghai, China). After incubation for 1 h at 37 °C, the absorbances were measured at 450 nm.

2.14. Measurement of lipid peroxides

Cells were seeded in 6-well plates and incubated with 5 μM C11-BODIPY (D3861, Thermo Fisher Scientific) in HBSS at 37 °C for 30 min. The cells were then washed twice with PBS, digested with trypsin to obtain cell pellets, and suspended in 500 μL of serum-free medium. Flow cytometric analysis was performed with an ID7000™ Spectral Cell Analyzer (Sony Biotechnology) and analyzed using FlowJo software (Treestar).

The relative MDA concentration in the cell lysate was determined using a Lipid Peroxidation Assay Kit (S0131S, Beyotime) according to the manufacturer's instructions. Briefly, 5×10^6 EC EC cells were seeded in 10-cm dishes and treated with erastin, RSL3, or DMSO for 12 h. Subsequently, the medium was discarded, and the cells were washed twice with PBS. Cell lysates were prepared using a standard cell lysis buffer for western blotting and immunoprecipitation (IP) (P0013, Beyotime). After centrifugation at 12,000 g for 10 min, 100 μl of supernatant was mixed with 200 μl of MDA working solution and incubated at 100 °C for 15 min. After cooling to room temperature, the absorbance of each mixture was measured at 532 nm.

2.15. Iron assay

Intracellular ferrous iron (Fe^{2+}) levels were determined using the iron assay Kit (ab83366, Abcam) according to the manufacturer's instructions. Cells (1×10^7) were harvested and lysed with buffer for western blotting and IP (P0013, Beyotime) after 12 h of treatment with

erastin, RSL3, or DMSO. The cell extracts were then centrifuged, and the supernatants were collected. Another centrifugation step (13,000 g, 10 min) at 4 °C was used to remove insoluble material. The supernatant was collected and an iron reducer was added to each sample before mixing and incubation at room temperature for 30 min. Next, 100 μL of the iron probe was added to the sample, mixed, and incubated for 1 h at room temperature in the dark. The absorbance at 593 nm was immediately measured using a colorimetric microplate reader.

Phen green SK (PGSK) (P14313, Invitrogen) is a fluorescent heavy metal indicator that can react with Fe^{2+}. PGSK emits fluorescence in living cells and quenched in the presence of Fe^{2+}, which can be used as a LIP probe as previously described [20].

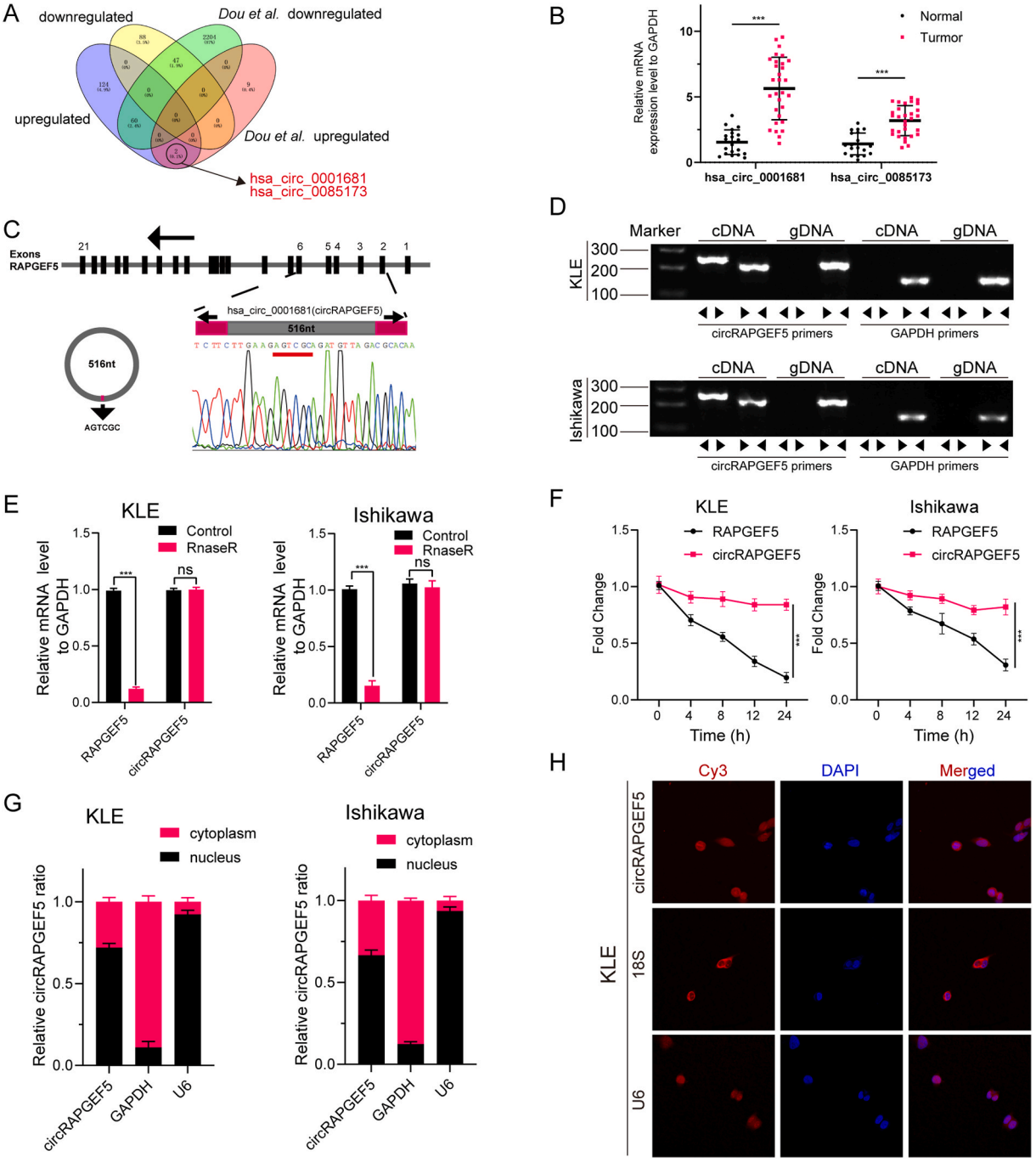

Fig. 1. Identification and characterization of circRAPGEF5 in EC.
(A) The Venn diagram shows common differential expressed genes between our sequencing results and results identified by Dou et al. **(B)** qRT-PCR validation of two co-overexpressed circRNAs in EC samples. **(C)** Scheme illustrating the production of circRAPGEF5. The back splicing junction was validated by Sanger sequencing. **(D)** The existence of circRAPGEF5 was validated in KLE and Ishikawa EC cells by PCR and agarose gel electrophoresis. GAPDH was used as a negative control. **(E)** The relative mRNA levels of circRAPGEF5 and RAPGEF5 were analyzed by qRT-PCR in KLE and Ishikawa cells treated with or without RNase R. Data were presented as the mean ± S.D. ns, not significant, ***P < 0.001 (Student's t-test). **(F)** qRT-PCR was conducted to determine the relative mRNA levels of circRAPGEF5 and RAPGEF5 after treatment with Act D at the indicated time points. ***P < 0.001 (one-way ANOVA). **(G)** Nucleoplasm and cytoplasm were separated to measure the expression levels of the circRAPGEF5, GAPDH and U6. **(H)** RNA FISH analysis of circRAPGEF5 localization in KLE cells. 18S and U6 were applied as positive controls.

2.16. Tumor xenograft model

All animal experiments were approved by the Animal Care Committee of the Tongji Medical College. Female 4-week-old BALB/c-nu nude mice were purchased from Vital River (Beijing, China) and housed in a specific pathogen-free facility. EC cells were washed twice with serum-free medium and injected subcutaneously into nude mice (5×10^6 cells/site). Tumors were measured with calipers every four days for four weeks. The mice were sacrificed on day 32 after cell implantation, and the tumors were excised and weighed.

2.17. Statistics

Data are expressed as mean ± SD. The means of the groups were compared using the Student's t-test and ANOVA, as indicated in the figure legends. Statistical analyses were performed using Prism 8.1.2 (GraphPad Software Inc.).

3. Results

3.1. Identification and characterization of circRAPGEF5 in endometrial cancer

To identify potential candidates that promote EC progression, we analyzed the expression profile of circRNAs in five pairs of human EC and normal tissues using high-throughput sequencing. As a result, 323 circRNAs were differentially expressed according to fold-change (FC) filtering ($|\log_2 FC| > 1$) and $P < 0.05$. Among them, 136 circRNAs were significantly upregulated while 187 were significantly downregulated in the EC tissues (Supplementary Table S2). We then explored the intersection between common differentially expressed circRNAs, previously identified by Dou et al., with our differentially expressed circRNAs [21]. Finally, we obtained two commonly upregulated circRNAs, hsa_circ_0001681 and hsa_circ_0085173 (Fig. 1A), and examined their expression levels in clinical EC specimens (EC = 30, normal = 25) using RT-qPCR. The most prominent upregulated circRNA was hsa_circ_0001681 (termed circRAPGEF5) (Fig. 1B). Simultaneously, statistical analysis demonstrated that high expression of circRAPGEF5 significantly and positively correlated with clinicopathological features, including FIGO stage and histological grade in EC patients (Table 1). CircRAPGEF5 was derived from regions in exons 2, 3, 4, 5, and 6 within the RAPGEF5 locus, comprising 516 nucleotides (nt) (Fig. 1C). RAPGEF5 serves as a RAS activator by promoting the acquisition of GTP to maintain the active GTP-bound state and is the key link between cell surface receptors and RAS activation [22]. To investigate the function of circRAPGEF5 in cell biological behavior, we determined its expression levels with qRT-PCR in various EC cell lines. The results showed that circRAPGEF5 expression was relatively high in KLE and comparatively low in Ishikawa (Supplementary Fig. 1A). The KLE and Ishikawa cells were selected for further investigation.

PCR amplification was performed to obtain the putative back-spliced junction fragment of circRAPGEF5, using divergent primers from cDNA, which was further confirmed by Sanger sequencing (Fig. 1C). The cDNA and genomic DNA (gDNA) were then amplified using convergent and divergent primers, respectively. Gel electrophoresis indicated that circRAPGEF5 could be amplified by divergent primers in cDNA, but not in gDNA (Fig. 1D). The RNase R exonuclease assay and RT-qPCR results were indicative of the stability of circRAPGEF5 compared to linear RNA (Fig. 1E). Moreover, circRAPGEF5 transcripts degraded at a slower rate than linear RAPGEF5 mRNA transcripts upon treatment with Act D (Fig. 1F). FISH and a cytoplasmic and nuclear RNA isolation assay indicated that circRAPGEF5 was mainly distributed in the nucleus of EC cells (Fig. 1G and H, and Supplementary Fig. 1B).

3.2. CircRAPGEF5 promotes EC cell proliferation in vitro and in vivo

To investigate the role of circRAPGEF5 in EC cells, loss- and gain-of-function studies were performed. First, lentiviral shRNA, against the back-splicing of circRAPGEF5, was stably integrated into KLE cells, and the circRAPGEF5 overexpression lentivirus was stably integrated into Ishikawa cells. A qRT-PCR confirmed the transfection efficacy of lentivirus (Supplementary Fig. 2A). As shown in Supplementary Figs. 2B and C, knockdown or overexpression of circRAPGEF5 had no impact on the expression of RAPGEF5 at the mRNA and protein levels. CCK8, clone formation, and EdU incorporation assays revealed that knockdown of circRAPGEF5 significantly inhibited the proliferation of EC cells, whereas overexpression facilitated EC proliferation in vitro (Fig. 2A–D). To further investigate the effects of circRAPGEF5 in vivo, we established subcutaneous xenograft tumor models in female BALB/c nude mice. Knockdown of circRAPGEF5 significantly suppressed tumor growth in vivo, whereas circRAPGEF5 overexpression enhanced tumor growth in vivo, as measured by the tumor growth curve and weights (Fig. 2E–G). These results demonstrate that circRAPGEF5 exerts growth-promoting effects on EC cells in vitro and in vivo, suggesting that it serves an important oncogenic function in EC progression.

3.3. circRAPGEF5 interacts with RBFOX2 protein in EC cells

It has been reported that circRAPGEF5 regulates miRNA expression by functioning as a sponge [23]. Therefore, we assessed whether circRAPGEF5 could sponge miRNAs to promote EC progression. Since AGO2 is the primary mediator of circRNA–miRNA interactions [24], RIP experiments were conducted in EC cell extracts using an AGO2 antibody. The results showed no detectable enrichment of circRAPGEF5 in the AGO2 antibody group compared to the IgG control group (Supplementary Fig. 3A). Furthermore, CLIP analysis for AGO2 revealed the absence of circRAPGEF5 binding [25]. To explore whether circRAPGEF5 might exert its function through protein binding, we performed RNA pull-down with biotinylated probes targeting the circRAPGEF5 back-spliced sequence. Specific probe-bound proteins were examined by silver staining and identified using mass spectrometry. The RNA-binding protein RBFOX2 was identified as a circRAPGEF5-associated protein (Fig. 3A, Supplementary Fig. 3B, and Supplementary Table S3). The interaction between circRAPGEF5 and RBFOX2 was further validated by an RNA pull-down assay and RIP/qRT-PCR analysis (Fig. 3B and C). To confirm this result, we used IF and FISH assays to demonstrate that the endogenous circRAPGEF5 is co-localized with RBFOX2 in EC cells (Fig. 3D).

The RBFOX2 protein consists of an RNA recognition motif (RRM) and a C-terminal of Fox-1 domain (Fox-1 C-terminal domain) across the structure. To identify the domain required for interactions with circRAPGEF5, full-length, and a variety of truncated forms of, RBFOX2 were overexpressed in EC cells. CircRAPGEF5 was predicted to bind to the Fox-1 C-terminal domain using the catRAPID algorithm (Fig. 3E) [26]. An anti-Flag RIP assay also illustrated that the Fox-1 C-terminal domain (266–367 amino acids) was responsible for the interaction with circRAPGEF5 (Fig. 3F and G and Supplementary Figs. 3C and D). In summary, these results suggest that, in EC cells, circRAPGEF5 forms an RNA-protein complex with RBFOX3 through the Fox-1 C-terminal domain.

3.4. circRAPGEF5 modulates alternative splicing via RBFOX2

To further investigate whether circRAPGEF5 could alter the expression of RBFOX2, we measured its expression levels at both the mRNA and protein levels. Overexpression or knockdown of circRAPGEF5 had no effect on the mRNA and protein levels of RBFOX2 (Supplementary Figs. 4A and B). Meanwhile, no significant difference in circRAPGEF5 expression was found between the RBFOX2-knockdown and control cells (Supplementary Figs. 4C and D). Collectively, these

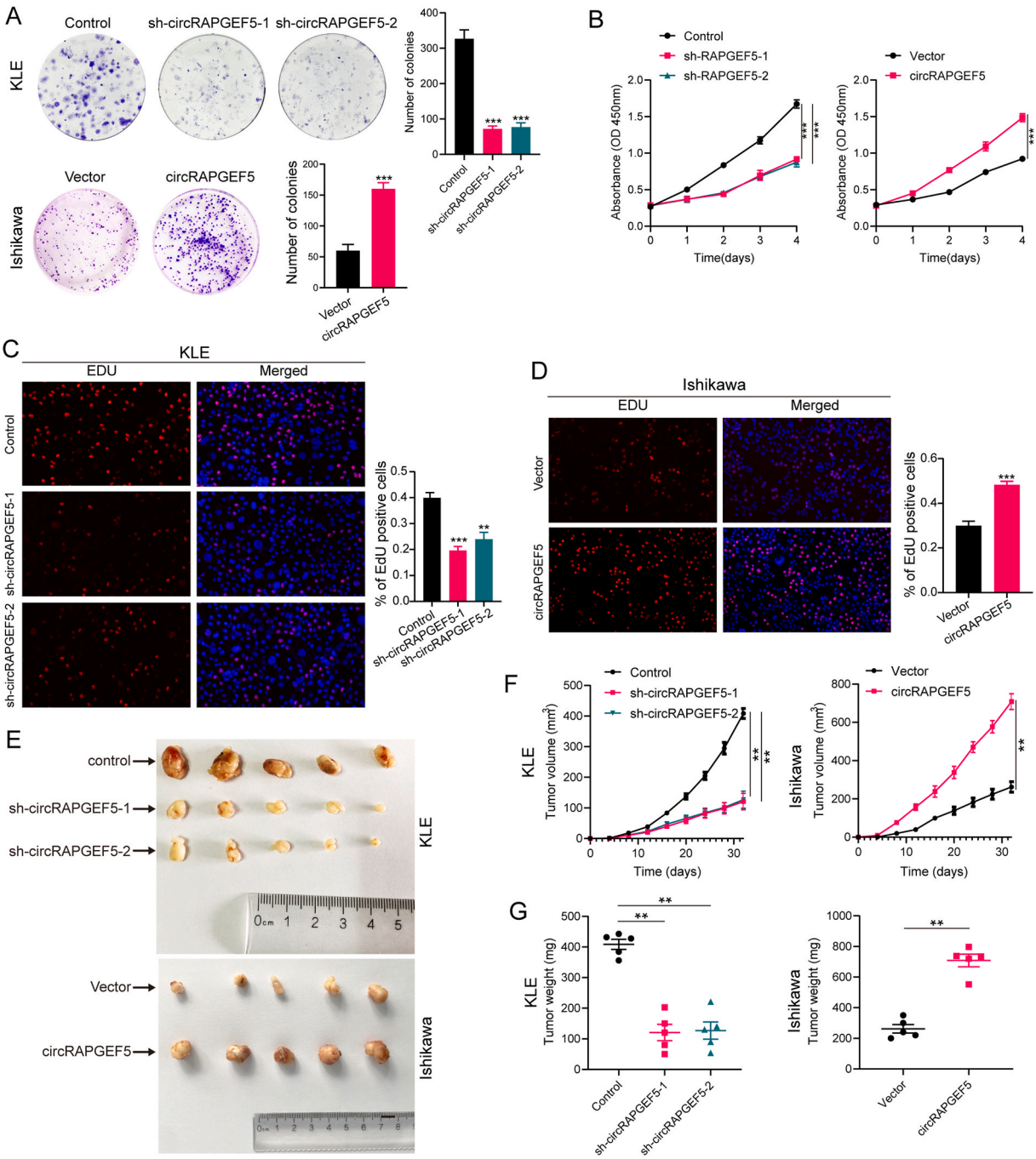

Fig. 2. CircRAPGEF5 enhances EC cells proliferation in vitro and in vivo.
(A) clone formation, **(B)** CCK8 assay and **(C, D)** EdU incorporation assay were conducted to determine the EC cells proliferation in vitro. KLE cells were stably transfected with control, sh-circRAPGEF5-1 or sh-circRAPGEF5-2 lentivirus. Ishikawa cells were stably transfected with empty vectors or circRAPGEF5 overexpression lentivirus. **(E)** Representative images of xenograft tumors at the endpoint. **(F)** Growth curve of subcutaneous xenograft tumor in mice injected with indicated EC cells. **(G)** Weights of the xenograft tumors were measured and the results are shown in the scatterplot. Data were mean ± SD. **P < 0.01, ***P < 0.001 (Student's t-test).

results suggest that circRAPGEF5 may regulate EC cell proliferation by affecting the RBFOX2 protein activity, rather than expression.

As an RBP, RBFOX2 controls the splicing of a large number of transcripts involved in cell differentiation and development [27]. RBFOX2 has been implicated in the development of ovarian and breast cancer, as well as the epithelial to mesenchymal transition [28–30]. However, it is uncertain whether circRAPGEF5 exerts its effect by regulating critical AS events in an RBFOX2-dependent manner. In this regard, we performed nanopore sequencing on circRAPGEF5 knockdown KLE and sh-controlled KLE cells. CircRAPGEF5 knockdown resulted in 727 AS events in KLE cells, including 139 skipping exons (SE) (Fig. 4A). Gene ontology analysis for AS event-related genes indicated an association with biological processes involved in protein metabolism, oxidative phosphorylation, mRNA splicing, lipid metabolism, and metal ion SLC transporters (Fig. 4B). To validate whether the circRAPGEF5/RBFOX2 complex could regulate AS events in EC cells, we examined splicing variants using RT-PCR with primer pairs spanning specific exons for six genes (Supplementary Table 1). These results confirmed that

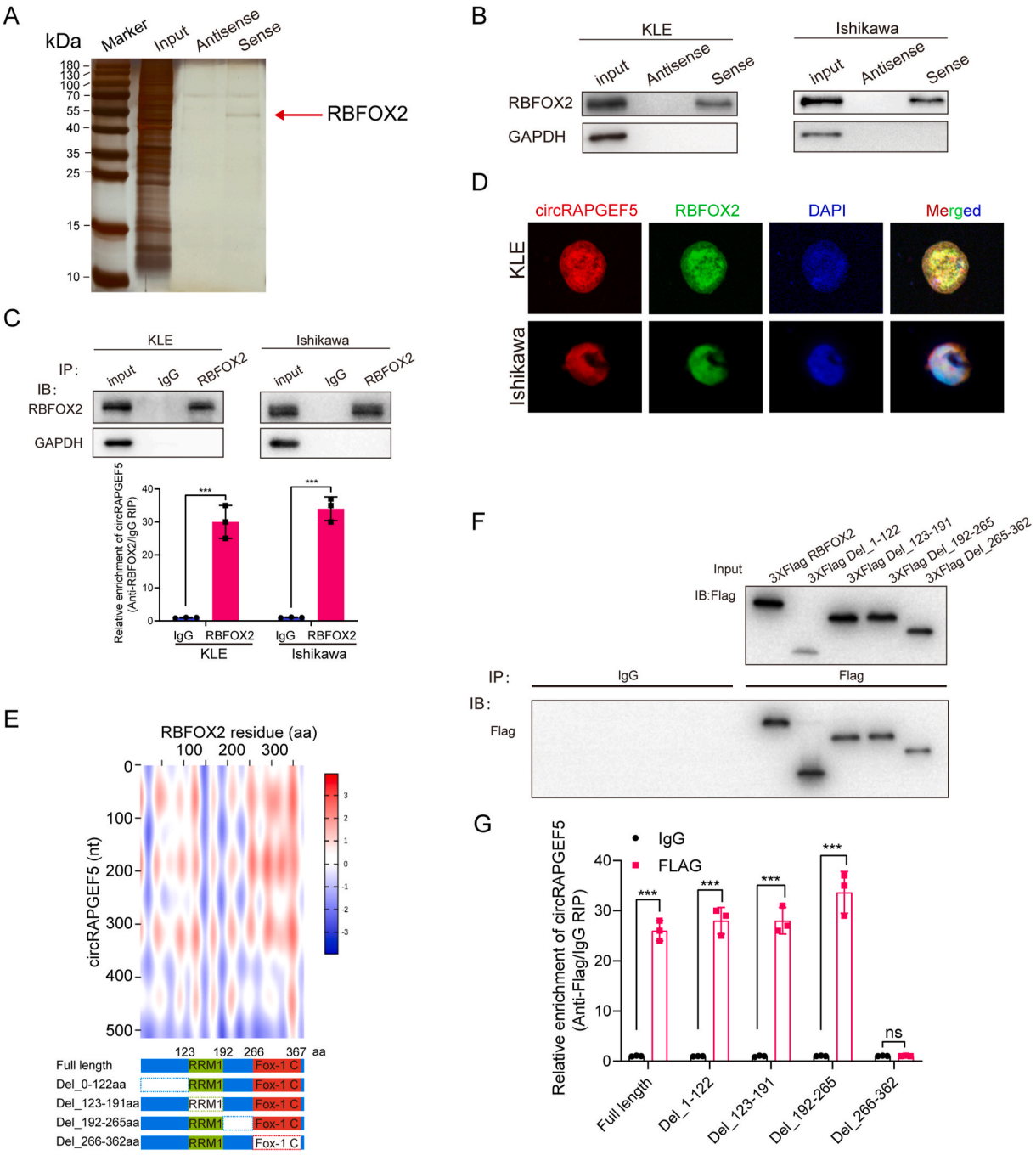

Fig. 3. CircRAPGEF5 binds to RBFOX2 protein.
(A) RNA pull-down was performed using the biotin-labeled sense or antisense probes in the KLE cell. Bound proteins were analyzed by SDS–PAGE and silver staining. **(B)** RBFOX2 immunoblot analysis of sense and antisense circRAPGEF5 RNA pull-downs in KLE and Ishikawa cells. GAPDH was used as the loading control. **(C)** RIP assays in KLE and Ishikawa cells using RBFOX2 and IgG antibody. The precipitate was subjected to western blotting with antibodies against the indicated proteins. The relative levels of circRAPGEF5 enriched by RBFOX2 or IgG were determined by qRT-PCR. **(D)** FISH combined with IF staining were performed to determine colocalization of circRAPGEF5 and RBFOX2. **(E)** The catPAPID algorithm was used to predict the circRAPGEF5-RBFOX2 interaction. Schematic diagram illustrating full-length RBFOX2 and truncated forms of RBFOX2. **(F)** KLE cells were transfected with 3 × Flag-RBFOX2 full-length or truncations, which were determined by Western blot with an anti-FLAG antibody. **(G)** The relative enrichment of endogenous circRAPGEF5 in truncated RBFOX2 RIP was measured by qRT-PCR. Data were mean ± SD. ns, not significant, ***P < 0.001 (Student's t-test).

circRAPGEF5 can induce specific exon exclusion (TFRC, ANXA2, EIF5A, and ITGAE) and inclusion (SIKE1 and TSPO) (Fig. 4C). Interestingly, RBFOX2 regulates the AS of downstream genes in the opposite direction of circRAPGEF5.

It has been reported that non-coding RNA (ncRNA) may serve as a "decoy" by interacting directly with splicing factors and inhibiting these proteins from binding to pre-mRNAs, thereby influencing AS in cancers [31,32]. Given that circRAPGEF5 and RBFOX2 play opposing roles in regulating the AS of downstream genes, RIP/qRT-PCR assays were performed to investigate how circRAPGEF5 affects the binding affinity of RBFOX2 to pre-mRNAs of downstream target genes. As shown in Supplementary Fig. 4E, circRAPGEF5 knockdown significantly enhanced the RBFOX2 binding affinity in EC cells. Altogether, these results indicate that circRAPGEF5 modulates AS by sequestering

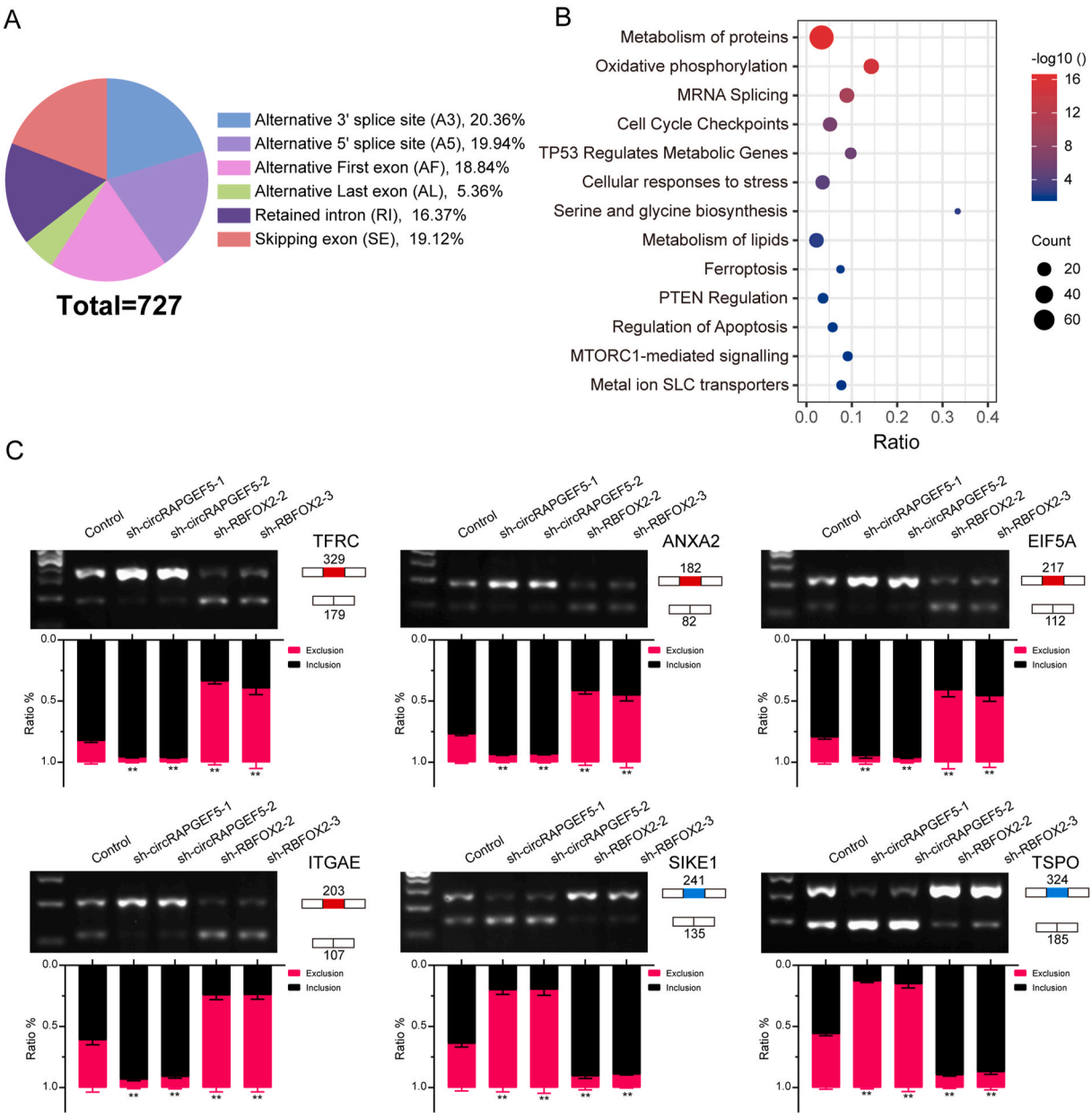

Fig. 4. The effects of CircRAPGEF5 and RBFOX2 on alternative splicing
(A) Number and proportion of different alternative splicing events after the circRAPGEF5 knockdown in KLE cells, as identified by the AStalavista tool. **(B)** Gene Ontology analysis for alternative splicing events related genes. **(C)** Representative circRAPGEF5 affected skipping exons was validated by using PCR and agarose gel electrophoresis upon knockdown of circRAPGEF5 or RBFOX2 in KLE cells. Data were mean ± SD, **P < 0.01 (Student's t-test).

RBFOX2.

3.5. *CircRAPGEF5 desensitized EC cells to ferroptosis via RBFOX2*

CircRAPGEF5-regulated AS was found to promote the exon-4 exclusion of TFRC by forming a truncated transcript. Moreover, gene ontology analysis for AS event-related genes revealed enrichment in the ferroptosis pathway. Ferroptosis is an iron-dependent non-apoptotic cell death that is characterized by intracellular iron disorder and accumulation of lipid peroxides in the cell membrane [33]. To determine whether circRAPGEF5 could affect cellular sensitivity to ferroptosis, EC cells were treated with the classic ferroptosis inducers, erastin and RSL3. The dose-response curves for erastin and RSL3 were generated, and half-maximal inhibitory concentrations (IC50) were calculated (Supplementary Figs. 5A–D). Therefore, KLE was treated with 15 μM erastin and 10 μM RSL3 and Ishikawa was treated with 10 μM erastin and 5 μM RSL3, for 12 h in all subsequent experiments. Interestingly, circRAPGEF5 knockdown increased, while circRAPGEF5 overexpression decreased, sensitivity of EC cells to erastin and RSL3 (Fig. 5A). Moreover, knockdown of circRAPGEF5 sensitized KLE cells to erastin-induced growth inhibition over time, which could be rescued by the chelator deferoxamine (DFO) but not by the apoptosis inhibitor Z-VAD-FMK or the autophagy inhibitor 3-MA (Fig. 5B and Supplementary Fig. 5E). In addition, we also examined the effect of circRAPGEF5 on cellular labile iron pool (LIP) and ferritin, a protein complex that chelates iron in cells. The results suggested that knockdown of circRAPGEF5 increased the free iron pool and lead to the reduction of ferritin, while overexpression of circRAPGEF5 decreased the free iron pool and lead to the increase of ferritin expression (Supplementary Fig. 6).

Consistently, in EC cells treated with erastin or RSL3, circRAPGEF5

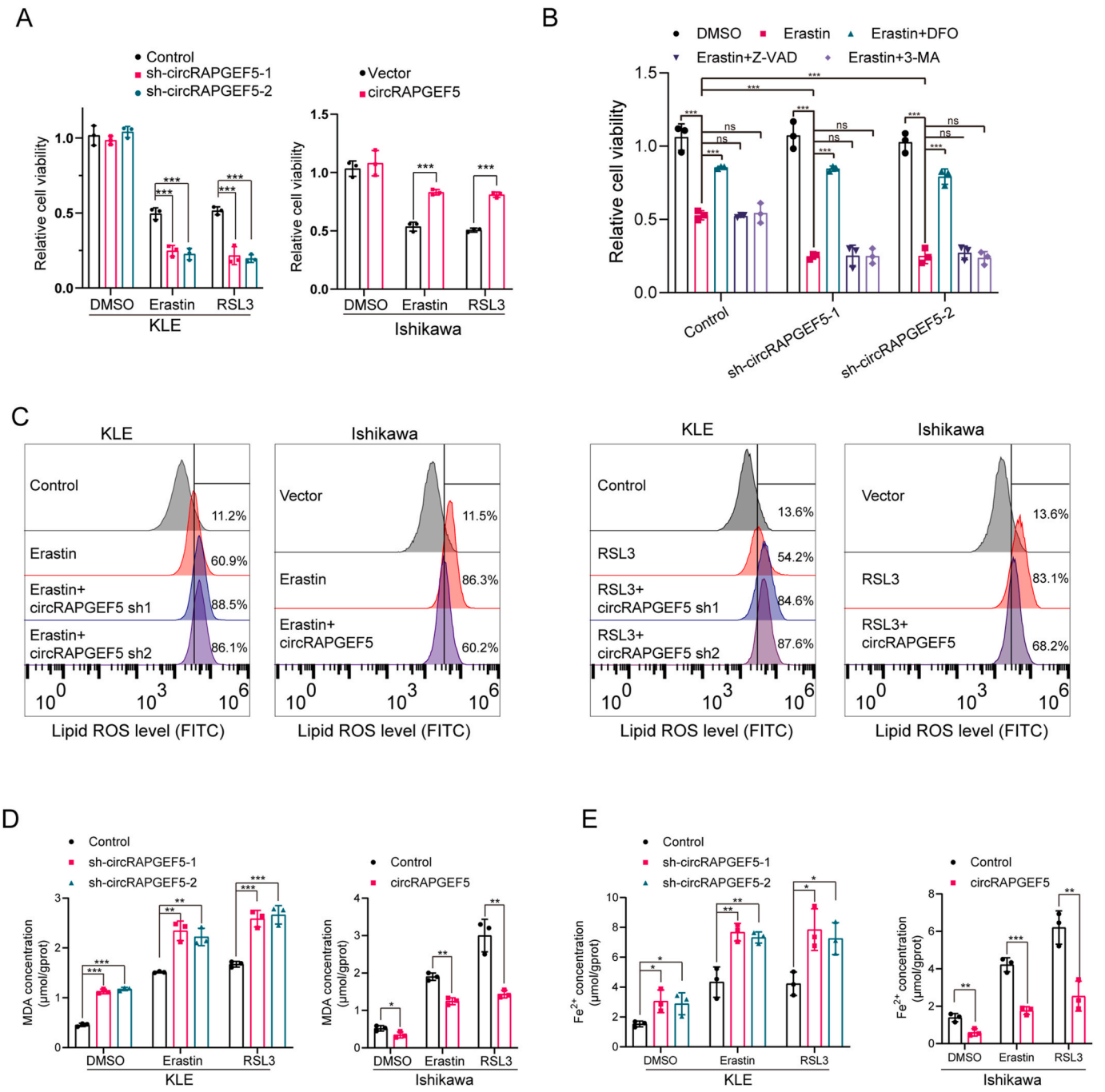

Fig. 5. CircRAPGEF5 suppressed erastin- and RSL3-induced ferroptosis
(A) Cell viability was assessed after treatment with erastin (KLE:15 μM, Ishikawa: 10 μM) and RSL3 (KLE:10 μM, Ishikawa: 5 μM) in circRAPGEF5-knockdown KLE cells and circRAPGEF5-overexpression Ishikawa cells. **(B)** The viability of circRAPGEF5-knockdown KLE cells treated with erastin combined with DFO, Z-VAD, or 3-MA. **(C)** Lipid ROS accumulation was analyzed by flow cytometry with C11-BODIPY staining. **(D)** Lipid peroxides were measured by MDA assay. **(E)** The intracellular Fe^{2+} was measured by iron detection assay. Data were mean ± SD. ns, not significant,**P < 0.01, (Student's t-test).

knockdown significantly increased lipid peroxidation levels, as determined by the C11-BODIPY staining and malondialdehyde (MDA) measurement. Whereas, overexpression of circRAPGEF5 decreased extracellular lipid peroxidation levels (Fig. 5C and D). Furthermore, we found that circRAPGEF5 knockdown resulted in an increase in intracellular iron under erastin and RSL3 treatment conditions and circRAPGEF5-overexpressing lead to the decreased intracellular iron levels in Ishikawa cells under the same treatment (Fig. 5E).

To further confirm that circRAPGEF5 functions in an RBFOX2-dependent manner, we performed a series of rescue experiments. RBFOX2 knockdown restored resistance to erastin and RSL3 in circRAPGEF5 knockdown KLE cells (Fig. 6A). Consistently, RBFOX2 knockdown attenuated the intracellular levels of MDA, Fe^{2+} and lipid ROS in circRAPGEF5 knockdown cells upon treatment with erastin and RSL3 (Fig. 6B–D). Alternately, we overexpressed RBFOX2 in circRAPGEF5-overexpressed Ishikawa cells and found that ferroptosis inducer-hyposensitivity, resulting from circRAPGEF5-overexpression, was partially restored by the upregulation of RBFOX2. Thus, intracellular levels of MDA, lipid ROS, and Fe^{2+} elevated accordingly (Supplementary Fig. 5F, Fig. 6E–G). Altogether, these results suggest that

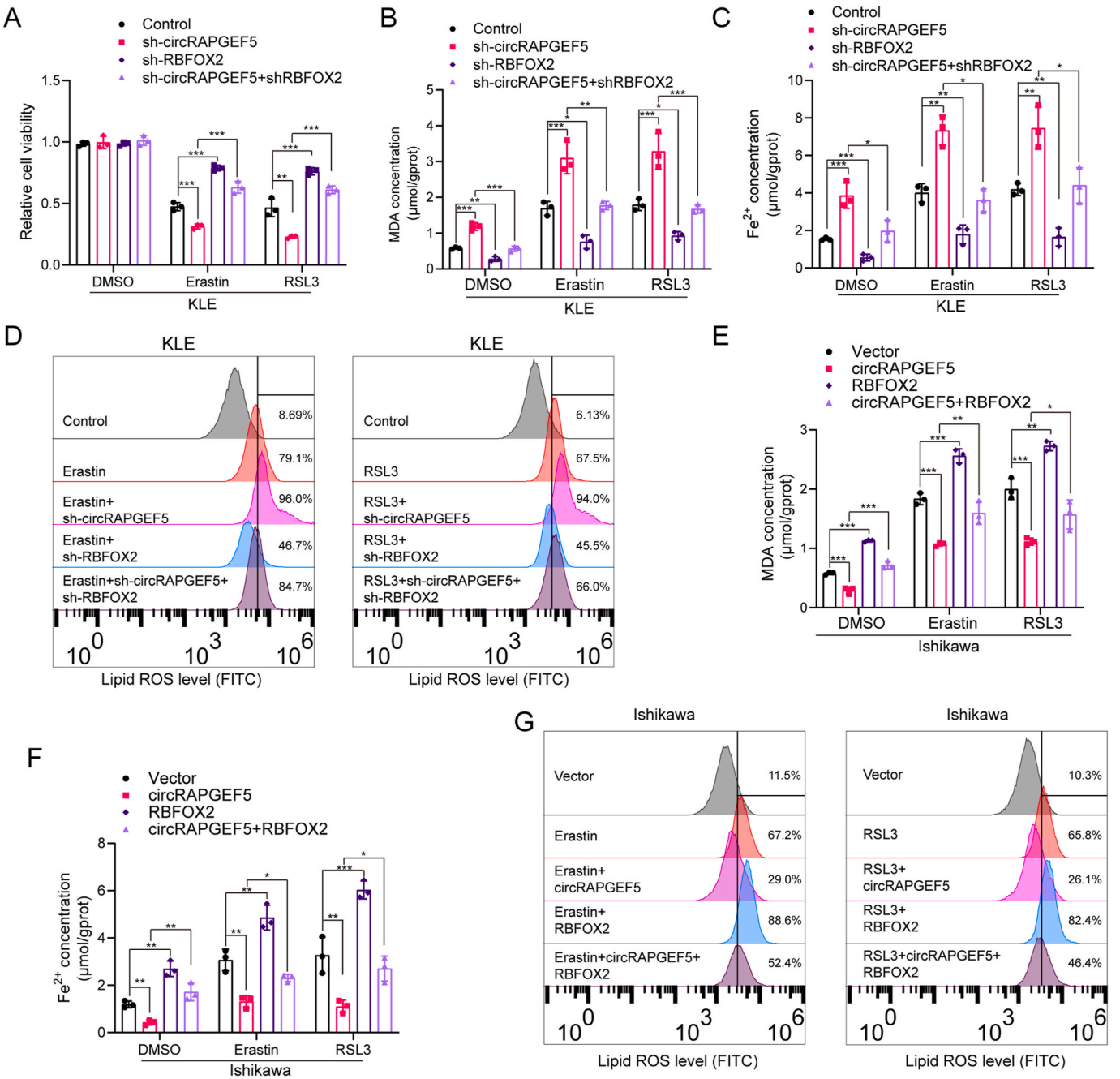

Fig. 6. CircRAPGEF5 confers EC cells insensitivity to ferroptosis via interaction with RBFOX2
(A) Cell viability was analyzed using a CCK-8 kit in KLE cells transfected with indicated constructs upon erastin or RSL3 treatment for 12 h. **(B)** Lipid peroxides were evaluated by MDA assay in KLE cells. **(C)** The intracellular Fe^{2+} was measured by iron detection assay in KLE cells. **(D)** Lipid ROS levels were determined by flow cytometry with C11-BODIPY staining in KLE cells. **(E)** Lipid peroxides were evaluated by MDA assay in Ishikawa cells transfected with indicated constructs upon erastin or RSL3 treatment for 12 h. **(F)** The intracellular Fe^{2+} was measured by iron detection assay in Ishikawa cells. **(G)** Lipid ROS levels were determined by flow cytometry in Ishikawa cells. Data were mean ± SD. *P < 0.05, **P < 0.01, ***P < 0.001 (Student's t-test).

circRAPGEF5 confers resistance to ferroptosis in EC cells by obstructing the binding of RBFOX2 to the TFRC pre-mRNA.

3.6. circRAPGEF5 promotes resistance to ferroptosis by regulating the alternative splicing of TFRC

Since the fourth exon deletion of TFRC can cause altered protein-coding sequence, the translated products of the truncated TFRC may be completely different from that of the wild-type TFRC, which leads to its inability to localize to the cell membrane to transport irons. To confirm whether circRAPGEF5 promotes resistance to ferroptosis by regulating AS of TFRC, expression plasmids encoding full-length TFRC (TFRC-*L*) or fourth exon-deleted TFRC (TFRC-*S*), were constructed and transfected into circRAPGEF5-overexpressing Ishikawa cells (Fig. 7A). Compared to TFRC-*S*, TFRC-*L* isoform possessed a greater ability to recover susceptibility of circRAPGEF5-overexpressing EC cells to erastin and RSL3 (Fig. 7B). Meanwhile, the decreased levels of MDA, lipid ROS, and Fe^{2+} were partially restored by the overexpression of TFRC-*L*, but not overexpression of TFRC-*S* (Fig. 7C–E). Based on these results, we conclude that circRAPGEF5 functions as a decoy that perturbs the binding of RBFOX2 to TFRC pre-mRNA, and yields truncated TFRC-*S*, ultimately contributing to the resistance of ferroptosis in EC (Fig. 7F).

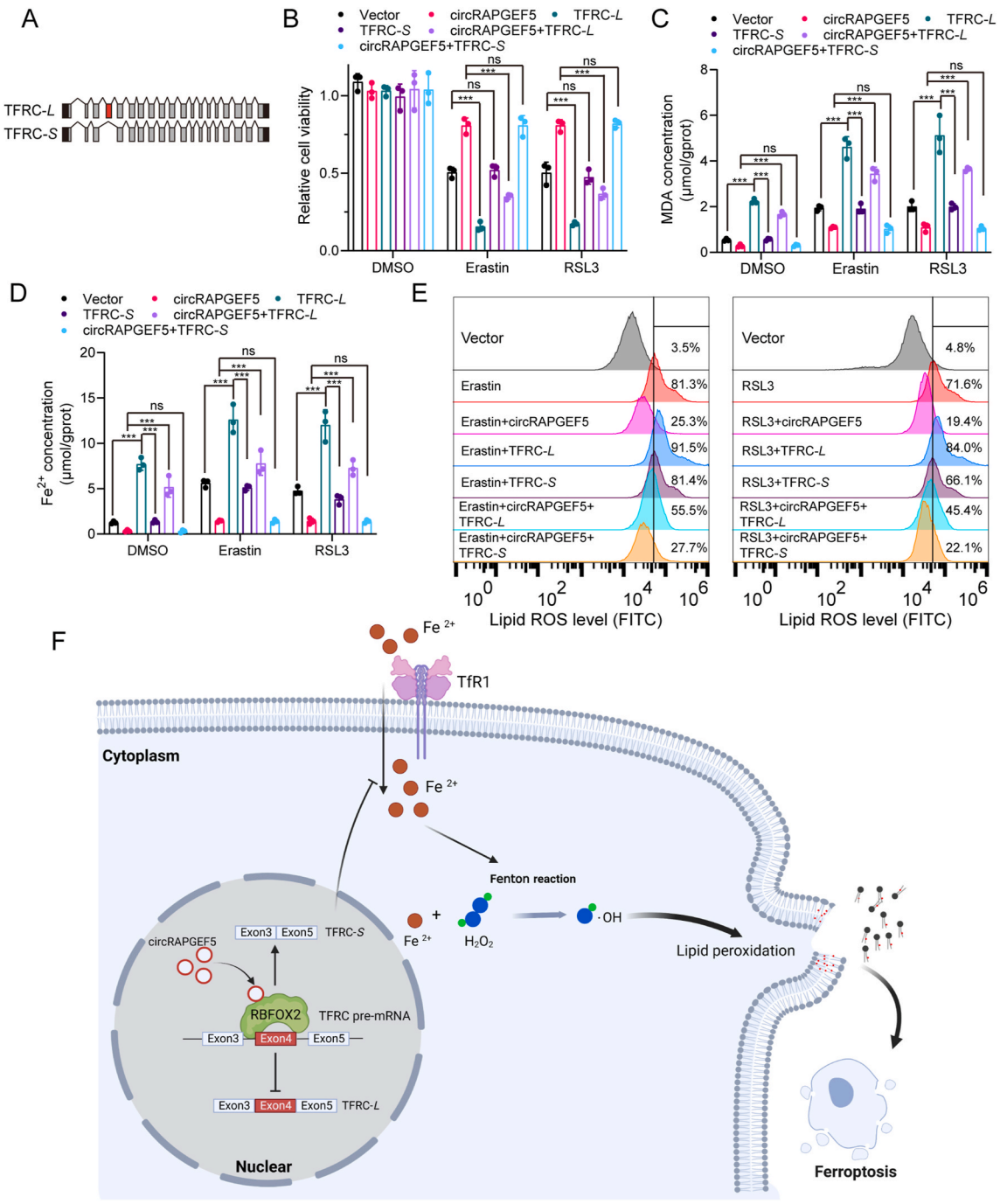

Fig. 7. CircRAPGEF5 confers EC cells insensitivity to ferroptosis through regulating the alternative splicing of TFRC
(A) Schematic diagram of TFRC splicing variants. The red box represents the alternative exon-4. **(B)** Cell viability was analyzed using a CCK-8 kit in Ishikawa cells transfected with empty vector control, circRAPGEF5, TFRC-*L*, TFRC-*S*, circRAPGEF5 + TFRC-*L*, ircRAPGEF5 + TFRC-*S*. **(C)** Lipid peroxidation was evaluated by MDA assay. **(D)** The intracellular Fe^{2+} was assessed in cells described in **(B)**. **(E)** Lipid ROS levels were detected by flow cytometry after incubation with C11-BODIPY in cells described in **(B)**. **(F)** Schematic diagram showing a proposed model for the interactions among circRAPGEF5, RBFOX2, and TFRC in EC. CircRAPGEF5 could bind to RBFOX2 protein in the nucleus, where it attenuated the binding of RBFOX2 with pre-mRNA of TFRC and led to the decrease of the labile iron pool and lipid peroxide production, which confers EC cells insensitivity to ferroptosis inducers. Data were mean ± SD. ns, not significant,***P < 0.001 (Student's t-test). (For interpretation of the references to color in this figure legend, the reader is referred to the Web version of this article.)

4. Discussion

CircRNA maintains high intracellular expression levels, due to its stable structure, which suggests that it has important biological functions. Furthermore, there is increasing literature for the effects of circRNAs on the progression of various human diseases, including diabetes mellitus, neurological disorders, cardiovascular diseases, and cancer [12]. Several circRNAs have been reported to regulate ferroptosis. Specifically, HCC cells treated with sorafenib (SF) showed high expression levels of hsa_circ_0008367 (cIARS), which can inhibit autophagy by suppressing ALKBH5-mediated ferroptosis [34]. In the lung adenocarcinoma (LUAD), circP4HB has been found to be highly expressed, protecting LUAD from ferroptosis via modulation of the miR-1184/SLC7A11 axis [35]. In this study, we found that circRAPGEF5

is significantly upregulated in endometrial cancer and primarily localized in the nucleus. Gain-of-function and loss-of-function studies revealed that circRAPGEF5 promotes proliferation and resistance to ferroptosis in EC cells. Mechanistically, circRAPGEF5 exhibited pro-tumor effects by modulating the RBFOX2 splicing activity toward TFRC pre-mRNA. Our results demonstrate that circRAPGEF5 can bind directly to the Fox-1 C-terminal domain of the RBFOX2 protein, dramatically reducing the RBFOX2 binding to pre-mRNAs of downstream genes.

More than 1000 RBPs in the nucleus involved in the regulation of AS for pre-mRNA have been documented [36]. AS is spatiotemporal and varies depending on cell type, growth and development stages, and disease progression, leading to differing splicing patterns [37,38]. RBFOX2 belongs to the RBFOX family, and growing evidence indicates that RBFOX2 regulates AS in various tumors. Chun et al. reported that RBFOX2 binds to a GGAA motif in exon-7 and promotes its inclusion in forming GOLIM4-L in nasopharyngeal carcinoma (NPC) [39]. RBFOX2 was also found to mediate exon-11 inclusion in the insulin receptor pre-mRNA splicing in hepatoma cells [40]. Hilmar et al. revealed that RBFOX2 can regulate the splicing of MALT1, a protease from the BCR/NF-κB pathway [41]. In this study, we showed that, in EC, RBFOX2 functions as a key regulator for the splicing of the genes: TFRC, ANXA2, EIF5A, ITGAE, SIKE1, and TSPO. Moreover, circRAPGEF5 attenuates RBFOX2 splicing activity toward these target genes by binding to this protein, thereby leading to the formation of isoforms that promote tumor progression. However, the exact interaction between RBFOX2 protein and TFRC pre-mRNA needs to be further investigated, which may indicate the specific mechanisms by which circRAPGEF5 inhibits the splicing activity of RBFOX2.

The involvement of ncRNA in AS has been reported, previously [42,43]. Long non-coding RNA (lncRNAs), NEAT1 and NEAT2, regulate the phosphorylation status of splicing factors and result in AS events [44,45]. CircSMARCA5 binds to SRSF1, thereby decreasing the expression of the proangiogenic splicing isoform VEGF-Axxxa, and contributing to the repression of cancer progression in glioblastoma multiforme [46]. Similarly, a recent investigation revealed that circURI1 interacts with hnRNPM to inhibit metastasis by modulating the AS of VEGFA in gastric cancer [32]. Our research on the regulation of AS for TFRC by circRAPGEF5 also furthers understanding of the role circRNAs play in cancer progression. Nevertheless, the biological implications of circRAPGEF5 in regulating the AS of ANXA2, EIF5A, ITGAE, SIKE1, and TSPO need to be further elucidated.

Iron plays a crucial role in cell fate decisions during cell growth and survival. Through Fenton reactions, iron acts as a catalyst for lipid peroxidation during ferroptosis [47]. Ferroptosis is a recently discovered type of programmed cell death characterized by an intracellular iron disorder and accumulation of lipid peroxides [48]. TFRC encodes transferrin receptor protein 1 (TfR1), which is the primary cellular iron transporter [49]. In addition, numerous studies have shed light on the role of TFRC in regulating the ferroptosis sensitivity of cancer cells. Lu et al. reported that MYCN increases iron uptake and promotes the accumulation of labile iron pool and reprograms the cellular iron metabolism by upregulating the expression of TFRC [50]. Ye et al. revealed that an interaction between the YTHDF1 methyltransferase domain and TRFC mRNA's 3′UTR and 5′UTR leads to positive regulation of TFRC translation, which enhances iron metabolism in head and neck squamous cell carcinomas [51]. Guo et al. found that E3 βTrCP facilitates TFRC ubiquitination in a TRIB2-dependent manner and finally decreases labile iron in liver cancer cells [52]. However, the molecular regulation of TFRC in EC is still unclear. In the splicing patterns regulated by RBFOX2, our results demonstrate that TFRC is a critical factor affecting the fate of EC. CircRAPGEF5 promotes the formation of TFRC with exon-4 skipping by interfering with the binding of TFRC pre-mRNA to RBFOX2. The inability of TFRC-*S* to exert its normal iron transport function leads to a decrease in the intracellular labile iron pool and resistance to ferroptosis. The induction of ferroptosis is a promising therapeutic option for cancer therapy, and an increasing number of studies have focused on restoring the sensitivity of tumor cells to ferroptosis. Hamed et al. reported that MYCN causes massive lipid peroxidation upon decreases in cysteine, essential amino acid for glutathione (GSH) biosynthesis, and induces ferroptosis in neuroblastoma cells. Importantly, a combination of different ferroptosis inducers is able to achieve complete remission of neuroblastoma [53]. Jia et al. found that OTUD1 promotes TFRC-mediated iron transport by deubiquitinating and stabilizing IREB2, resulting in increased ROS production and ferroptosis [54]. Daniel reported that the repression of GST1 promotes a catabolic state and represses mitochondrial respiration. Thus, autophagy increases labile iron availability, which enhances ferroptotic stimulation [55]. Junmei et al. found that human cancer cells are resistant to ferroptosis when the PI3K function is activated or when PTEN is lost, which are ubiquitous features for human cancers, and that cancer cells are usually vulnerable to ferroptosis when the PI3K-AKT-mTOR signals are blocked [56]. Indeed, the PI3K-AKT-mTOR pathway is frequently dysregulated in EC [57], and most EC displays PTEN gene inactivation, which can be found in up to 83% of endometrioid tumors [58]. Our findings are in line with those of Junmei et al., where EC cells exhibited greater resistance to ferroptosis. Based on the results, circRAPGEF5 could desensitize EC cells to ferroptosis by sequestering RBFOX2. Therefore, we believe that this may be a novel mechanism underlying resistance to ferroptosis in EC cells and suggest that circRAPGEF5 could serve as a potential therapeutic target for EC.

5. Conclusions

In this study, we discovered that circRAPGEF5, a circRNA derived from the circularization of RAPGEF5, was significantly upregulated in EC. Further studies revealed that circRAPGEF5 interacts with RBFOX2, an important splicing regulator, to modulate the splicing of TFRC pre-mRNA. Importantly, circRAPGEF5 promotes exon-4 skipping of TFRC by sequestering RBFOX2, resulting in resistance to ferroptosis via the reduction of labile iron in EC cells. We characterized the regulatory effect of circRAPGEF5 on the function of RBFOX2 and indicated that circRAPGEF5 and RBFOX2 may serve as promising therapeutic targets for EC.

Availability of data and materials

The datasets supporting the conclusions of this article are available with the article and its supplementary files.

Funding

This work was supported by the National Natural Science Foundation of China (81974409), the Young Scientists Fund of the National Natural Science Foundation of China (82002765).

Authors' contributions

JZ, SC, and SW designed and performed the majority of experiments. SC and RS performed CCK8 and EdU assays. RZ and WZ carried out the FISH, IF and animal experiments. QZ, TH and DF performed qRT-PCR and western blots. JZ, ZY and HW wrote and revised the manuscript. All authors read and approved the final manuscript.

Declaration of competing interest

The authors declare that they have no known competing financial interests or personal relationships that could have appeared to influence the work reported in this paper.

Data availability

Data will be made available on request.

Acknowledgments

The authors thank the Medical Subcenter of HUST Analytical & Testing Center in the flow cytometry data acquisition.

Appendix A. Supplementary data

Supplementary data to this article can be found online at https://doi.org/10.1016/j.redox.2022.102493.

References

[1] N.A.J. Ryan, et al., The proportion of endometrial tumours associated with Lynch syndrome (PETALS): a prospective cross-sectional study, PLoS Med. 17 (9) (2020), e1003263.
[2] N. Eritja, et al., Autophagy orchestrates adaptive responses to targeted therapy in endometrial cancer, Autophagy 13 (3) (2017) 608–624.
[3] G. Amadio, et al., Emerging drugs for endometrial cancer, Expet Opin. Emerg. Drugs 19 (4) (2014) 497–509.
[4] V. Makker, et al., Lenvatinib plus pembrolizumab in patients with advanced endometrial cancer, J. Clin. Oncol. 38 (26) (2020) 2981–2992.
[5] D. Miller, et al., Late-Breaking Abstract 1: randomized phase III noninferiority trial of first line chemotherapy for metastatic or recurrent endometrial carcinoma: a Gynecologic Oncology Group study, Gynecol. Oncol. 125 (3) (2012).
[6] T. Maniatis, B. Tasic, Alternative pre-mRNA splicing and proteome expansion in metazoans, Nature 418 (6894) (2002) 236–243.
[7] E. Wang, I. Aifantis, RNA splicing and cancer, Trends Cancer 6 (8) (2020) 631–644.
[8] S.E. Lee, et al., Alternative splicing in hepatocellular carcinoma, Cell Mol Gastroenterol Hepatol 10 (4) (2020) 699–712.
[9] C. Chang, et al., The aberrant upregulation of exon 10-inclusive SREK1 through SRSF10 acts as an oncogenic driver in human hepatocellular carcinoma, Nat. Commun. 13 (1) (2022) 1363.
[10] C. Luo, et al., SRSF2 regulates alternative splicing to drive hepatocellular carcinoma development, Cancer Res. 77 (5) (2017) 1168–1178.
[11] P. Popli, et al., Splicing factor SF3B1 promotes endometrial cancer progression via regulating KSR2 RNA maturation, Cell Death Dis. 11 (10) (2020) 842.
[12] L.S. Kristensen, et al., The biogenesis, biology and characterization of circular RNAs, Nat. Rev. Genet. 20 (11) (2019) 675–691.
[13] X. Li, L. Yang, L.L. Chen, The biogenesis, functions, and challenges of circular RNAs, Mol. Cell. 71 (3) (2018) 428–442.
[14] J.N. Vo, et al., The landscape of circular RNA in cancer, Cell 176 (4) (2019) 869–881 e13.
[15] T.L.H. Okholm, et al., Transcriptome-wide profiles of circular RNA and RNA-binding protein interactions reveal effects on circular RNA biogenesis and cancer pathway expression, Genome Med. 12 (1) (2020) 112.
[16] X. Wu, et al., A novel protein encoded by circular SMO RNA is essential for Hedgehog signaling activation and glioblastoma tumorigenicity, Genome Biol. 22 (1) (2021) 33.
[17] Y. Wang, L. Yin, X. Sun, CircRNA hsa_circ_0002577 accelerates endometrial cancer progression through activating IGF1R/PI3K/Akt pathway, J. Exp. Clin. Cancer Res. 39 (1) (2020) 169.
[18] J. Hu, et al., circSLC6A6 sponges miR-497-5p to promote endometrial cancer progression via the PI4KB/hedgehog Axis, J Immunol Res 2021 (2021), 5512391.
[19] R. Shi, et al., CircESRP1 enhances metastasis and epithelial-mesenchymal transition in endometrial cancer via the miR-874-3p/CPEB4 axis, J. Transl. Med. 20 (1) (2022) 139.
[20] X. Qin, et al., Ferritinophagy is involved in the zinc oxide nanoparticles-induced ferroptosis of vascular endothelial cells, Autophagy 17 (12) (2021) 4266–4285.
[21] Y. Dou, et al., Proteogenomic characterization of endometrial carcinoma, Cell 180 (4) (2020) 729–748, e26.
[22] J.F. Rebhun, A.F. Castro, L.A. Quilliam, Identification of guanine nucleotide exchange factors (GEFs) for the Rap1 GTPase. Regulation of MR-GEF by M-Ras-GTP interaction, J. Biol. Chem. 275 (45) (2000) 34901–34908.
[23] W. Liu, et al., circRAPGEF5 contributes to papillary thyroid proliferation and metastatis by regulation miR-198/FGFR1, Mol. Ther. Nucleic Acids 14 (2019) 609–616.
[24] S.W. Chi, et al., Argonaute HITS-CLIP decodes microRNA-mRNA interaction maps, Nature 460 (7254) (2009) 479–486.
[25] J.H. Li, et al., starBase v2.0: decoding miRNA-ceRNA, miRNA-ncRNA and protein-RNA interaction networks from large-scale CLIP-Seq data, Nucleic Acids Res. 42 (issue) (2014) D92–D97.
[26] F. Agostini, et al., catRAPID omics: a web server for large-scale prediction of protein-RNA interactions, Bioinformatics 29 (22) (2013) 2928–2930.
[27] D. Zhou, et al., RBFOX2 alters splicing outcome in distinct binding modes with multiple protein partners, Nucleic Acids Res. 49 (14) (2021) 8370–8383.
[28] J.P. Venables, et al., Cancer-associated regulation of alternative splicing, Nat. Struct. Mol. Biol. 16 (6) (2009) 670–676.
[29] C. Braeutigam, et al., The RNA-binding protein Rbfox2: an essential regulator of EMT-driven alternative splicing and a mediator of cellular invasion, Oncogene 33 (9) (2014) 1082–1092.
[30] I.M. Shapiro, et al., An EMT-driven alternative splicing program occurs in human breast cancer and modulates cellular phenotype, PLoS Genet. 7 (8) (2011), e1002218.
[31] A. Huang, et al., Circular RNA-protein interactions: functions, mechanisms, and identification, Theranostics 10 (8) (2020) 3503–3517.
[32] X. Wang, et al., CircURI1 interacts with hnRNPM to inhibit metastasis by modulating alternative splicing in gastric cancer, Proc. Natl. Acad. Sci. U. S. A. 118 (33) (2021).
[33] X. Chen, et al., Broadening horizons: the role of ferroptosis in cancer, Nat. Rev. Clin. Oncol. 18 (5) (2021) 280–296.
[34] Z. Liu, et al., Circular RNA cIARS regulates ferroptosis in HCC cells through interacting with RNA binding protein ALKBH5, Cell Death Dis. 6 (2020) 72.
[35] C.F. Pan, et al., CircP4HB regulates ferroptosis via SLC7A11-mediated glutathione synthesis in lung adenocarcinoma, Transl. Lung Cancer Res. 11 (3) (2022) 366–380.
[36] Y. Lee, D.C. Rio, Mechanisms and regulation of alternative pre-mRNA splicing, Annu. Rev. Biochem. 84 (2015) 291–323.
[37] L.T. Gehman, et al., The splicing regulator Rbfox2 is required for both cerebellar development and mature motor function, Genes Dev. 26 (5) (2012) 445–460.
[38] T.A. Clark, et al., Discovery of tissue-specific exons using comprehensive human exon microarrays, Genome Biol. 8 (4) (2007) R64.
[39] C.L. Luo, et al., RBFOX2/GOLIM4 splicing Axis Activates vesicular transport pathway to promote nasopharyngeal carcinogenesis, Adv. Sci. 8 (16) (2021), e2004852.
[40] T. Nakura, et al., Rbfox2 mediates exon 11 inclusion in insulin receptor pre-mRNA splicing in hepatoma cells, Biochimie 187 (2021) 25–32.
[41] H. Quentmeier, et al., RBFOX2 and alternative splicing in B-cell lymphoma, Blood Cancer J. 8 (8) (2018) 77.
[42] N. Romero-Barrios, et al., Splicing regulation by long noncoding RNAs, Nucleic Acids Res. 46 (5) (2018) 2169–2184.
[43] Y. Liu, et al., Noncoding RNAs regulate alternative splicing in Cancer, J. Exp. Clin. Cancer Res. 40 (1) (2021) 11.
[44] D.R. Cooper, et al., Long non-coding RNA NEAT1 associates with SRp40 to temporally regulate PPARgamma2 splicing during adipogenesis in 3T3-L1 cells, Genes 5 (4) (2014) 1050–1063.
[45] P. Malakar, et al., Long noncoding RNA MALAT1 promotes hepatocellular carcinoma development by SRSF1 upregulation and mTOR activation, Cancer Res. 77 (5) (2017) 1155–1167.
[46] D. Barbagallo, et al., CircSMARCA5 regulates VEGFA mRNA splicing and angiogenesis in glioblastoma multiforme through the binding of SRSF1, Cancers 11 (2) (2019).
[47] B. Hassannia, P. Vandenabeele, T. Vanden Berghe, Targeting ferroptosis to iron out cancer, Cancer Cell 35 (6) (2019) 830–849.
[48] S.J. Dixon, et al., Ferroptosis: an iron-dependent form of nonapoptotic cell death, Cell 149 (5) (2012) 1060–1072.
[49] P. Aisen, Transferrin receptor 1, Int. J. Biochem. Cell Biol. 36 (11) (2004) 2137–2143.
[50] Y. Lu, et al., MYCN mediates TFRC-dependent ferroptosis and reveals vulnerabilities in neuroblastoma, Cell Death Dis. 12 (6) (2021) 511.
[51] J. Ye, et al., YTHDF1-enhanced iron metabolism depends on TFRC m(6)A methylation, Theranostics 10 (26) (2020) 12072–12089.
[52] S. Guo, et al., TRIB2 desensitizes ferroptosis via betaTrCP-mediated TFRC ubiquitiantion in liver cancer cells, Cell Death Dis. 7 (1) (2021) 196.
[53] H. Alborzinia, et al., MYCN mediates cysteine addiction and sensitizes neuroblastoma to ferroptosis, Nat. Can. (Que.) 3 (4) (2022) 471–485.
[54] J. Song, et al., The deubiquitinase OTUD1 enhances iron transport and potentiates host antitumor immunity, EMBO Rep. 22 (2) (2021), e51162.
[55] D.M. Kremer, et al., GOT1 inhibition promotes pancreatic cancer cell death by ferroptosis, Nat. Commun. 12 (1) (2021) 4860.
[56] J. Yi, et al., Oncogenic activation of PI3K-AKT-mTOR signaling suppresses ferroptosis via SREBP-mediated lipogenesis, Proc. Natl. Acad. Sci. U. S. A. 117 (49) (2020) 31189–31197.
[57] B.M. Slomovitz, et al., Phase II study of everolimus and letrozole in patients with recurrent endometrial carcinoma, J. Clin. Oncol. 33 (8) (2015) 930–936.
[58] J.L. Hecht, G.L. Mutter, Molecular and pathologic aspects of endometrial carcinogenesis, J. Clin. Oncol. 24 (29) (2006) 4783–4791.